

GPI – Cryogenic Spectrograph Optics Performances

S. Thibault^{*a}, P. Vallée^b, E. Artigau^b, J. Maire^b, R. Doyon^b, J-F. Lavigne^c, J. Larkin^d

^aDépartement de physique, de génie physique and Centre d'optique, photonique et laser (COPL)
Université Laval, Québec, Québec, CANADA G1V 0A6

^bUniversité de Montréal, Département de physique, Montréal, Canada

^cINO (headquarters), 2740, rue Einstein, Quebec City, Canada

^dUniversity of California, Division of Astronomy 90095, Los Angeles, United States

ABSTRACT

The science instrument for GPI (Gemini Planet Imager) is a cryogenic integral field spectrograph based on a lenslet array. The integral field nature of the instrument allows for a full mapping of the focal plane at coarse spectral resolution. With such a data cube, artifacts within the PSF such as residual speckles can be suppressed. Additionally, the initial detection of any candidate planet will include spectral information that can be used to distinguish it from a background object: candidates can be followed up with detailed spectroscopic observations. The optics between the lenslet array and the detector are essentially a standard spectrograph with a collimating set of lenses, a dispersive prism and a camera set of lenses in a folded assembly. We generally refer to this optical set as the spectrograph optics. This paper describes the laboratory optical performances over the field of view. The test procedure includes the imaging performances in both non dispersive and dispersive mode. The test support equipments include a test cryostat, an illumination module with monochromatic fiber laser, a wideband light source and a test detector module.

Keywords: Planet imager, cryogenic, spectrograph, test, image quality

1. INTRODUCTION

The Gemini Planet Imager (GPI), currently under construction for the 8-m Gemini South telescope, is a high contrast adaptive optics instrument intended for direct imaging of extrasolar planets and circumstellar disks [1,2]. The science instrument is a cryogenic integral field spectrograph (IFS) based on a lenslet array. The integral field nature of the instrument allows for a full mapping of the focal plane at coarse spectral resolution.

The GPI output 2.8'' (square) image from the coronagraph is first reimaged on a lenslet array (about 200X200, 0.014'' sampling). The image plane is then dissected by a lenslet array producing an array of micro-pupils. The input focal ratio is such that there are at least 2 micro-lenses per λ/D , each micro-lens having a pitch 110 μ m. The micro-pupils are then re-imaged through an optical train (spectrograph optics) and disperse by a prism on NIR detector (2048X2048 pixels), the spacing of spectra on the detector is 4.5 pixels perpendicular to dispersion. The spectral image is reconstructed by integrating the signal of each micro-pupil spread on the detector. Non-common aberrations are still present in this design but they affect only the shape of individual micro-pupil PSFs, the integrated signal being hardly affected. One important implementation of this design is that there is a minimum contamination from one wavelength to another (wavelength crosstalk).

The spectrograph collimator consists of a refractive F/3.52 (including the square corners) and the spectrograph camera is also all refractive design with a F/5.89. The IFS is composed of 8 lenses, 3 cleartran, 4 BaF2 and 1 S-FTM16. All lenses have spherical only surfaces.

This paper describes the tested optical performances over the field of view of the spectrograph optics. The test procedure includes the imaging performances in both non dispersive and dispersive mode. The test support equipments include a test cryostat, an illumination module with monochromatic **fiber** laser, a wideband light source and a test detector module.

2. TEST SET-UP

The IFS optics was tested at cryogenic (~80 K) temperature in the H-band with the dispersion prism in place but without the lenslet array at the entrance focal plane. The latter was replaced by an array of 10x10 pinhole grids (100 μm pitch; see Figure 1) rotated by 26.5 degrees with respect to the detector to simulate the proper orientation of the lenslet array. A (square) cold stop was placed in front of the prism. The cold stop was also rotated by 26.5 degrees with respect to the detector.

The IFS optics was mounted on the subplate provided by UCLA. All tests were performed with a Hawaii-2 engineering grade detector (18 μm pixel pitch) mounted on a focussing stage provided by UCLA and controlled by a cryogenic stepper motor. The total course of the focussing stage was measured warm and found to be 390 μm . Since the detector has only 2 functional quadrants (on a diagonal), the complete optical tests were performed over two cryo-cycles, one in which the detector was rotated by 90 degrees in order to sample the other half of the field-of-view (FOV).

The whole optical assembly was mounted inside the UdeM cryo test chamber equipped with a Leybold 150 W cryocooler. The cryostat features a 25 mm diameter window immediately followed by a cold baffle (relatively long tube) feeding external light onto the pinhole grid. A diagram of the test set-up inside the cryo-chamber is shown in the figure 2.

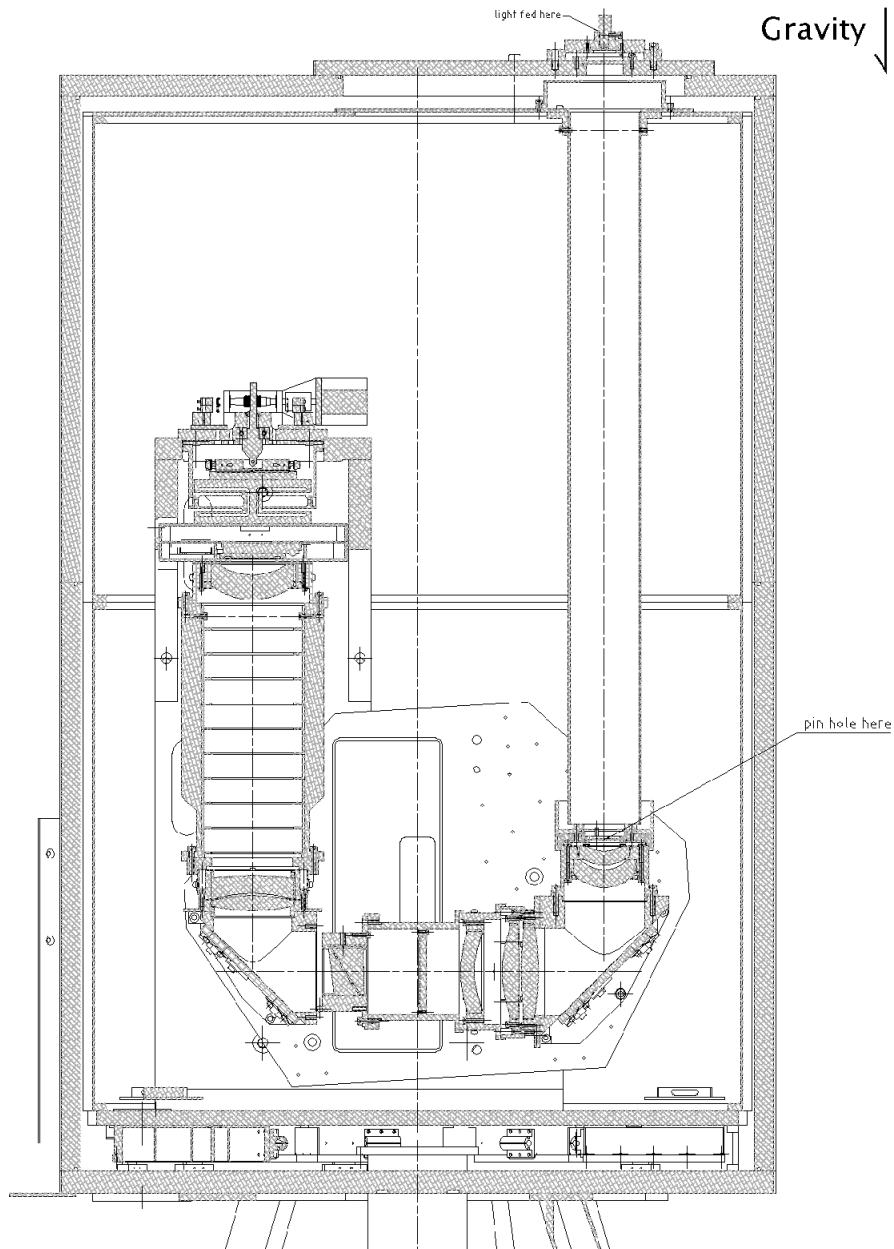


Figure 2: Diagram of the test set-up.

The following sources of light were used for the optical tests:

- A fiber-fed white light source (not spectrally uniform)
- A very narrow-band (a few nm) laser source at $1.55 \mu\text{m}$.
- Ar and Xe lamp
- Narrow-band filter at $1.644 \mu\text{m}$

A grid of pin-hole is placed in the object plane of the spectrograph. The object plane is located at the focal plane of the lenslet array. The figure 3 shows the drawing of the test patterns. It consists of several group of 10X10 pinholes with 100 um pitch which cover the entire spectrograph field of view. Each pinhole has a diameter of 5um (-0, +3um).

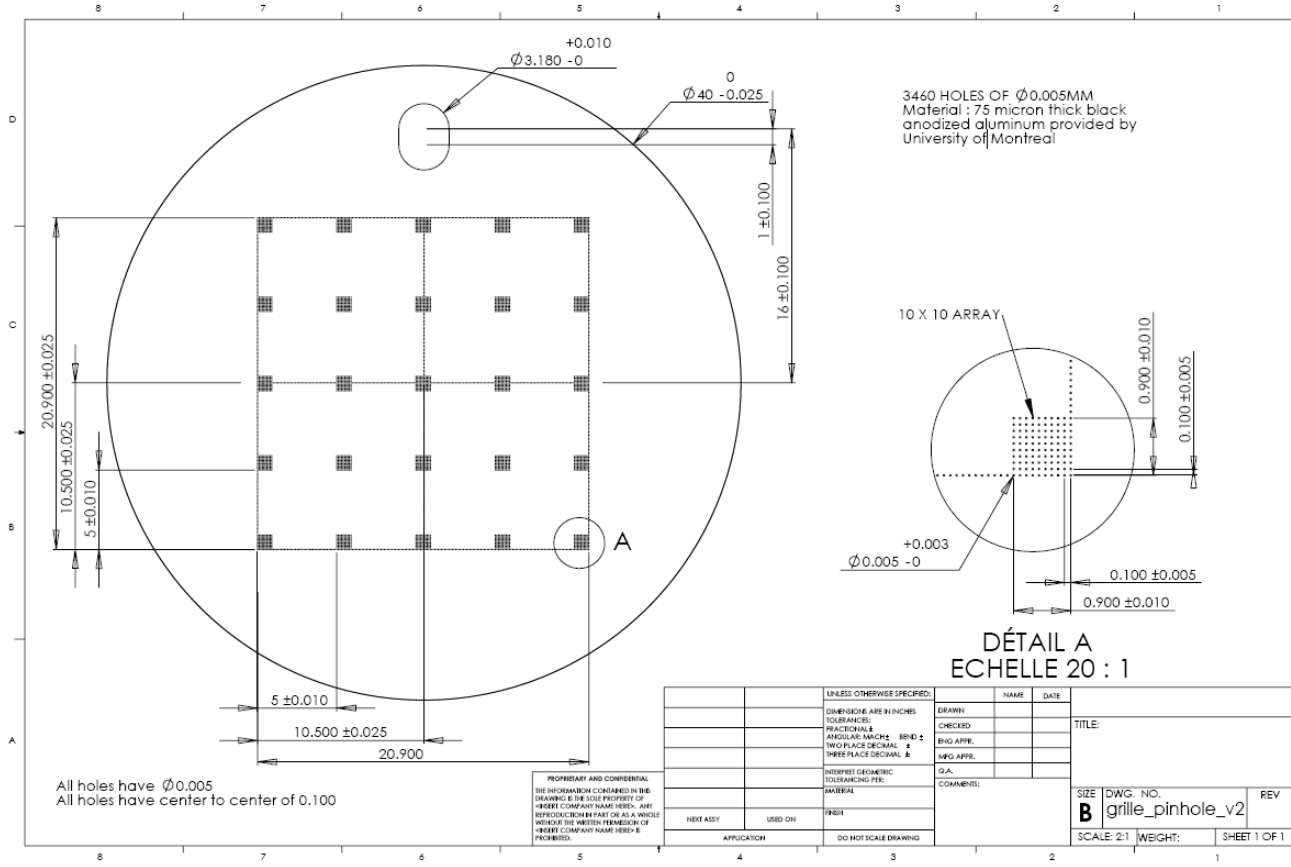


Figure 3: Detailed specifications of the pinholes mask used.

Locations of the 10x10 pinhole grids sampled over the full FOV (obtained over separate cryo-cycles) are labelled in the figure below.

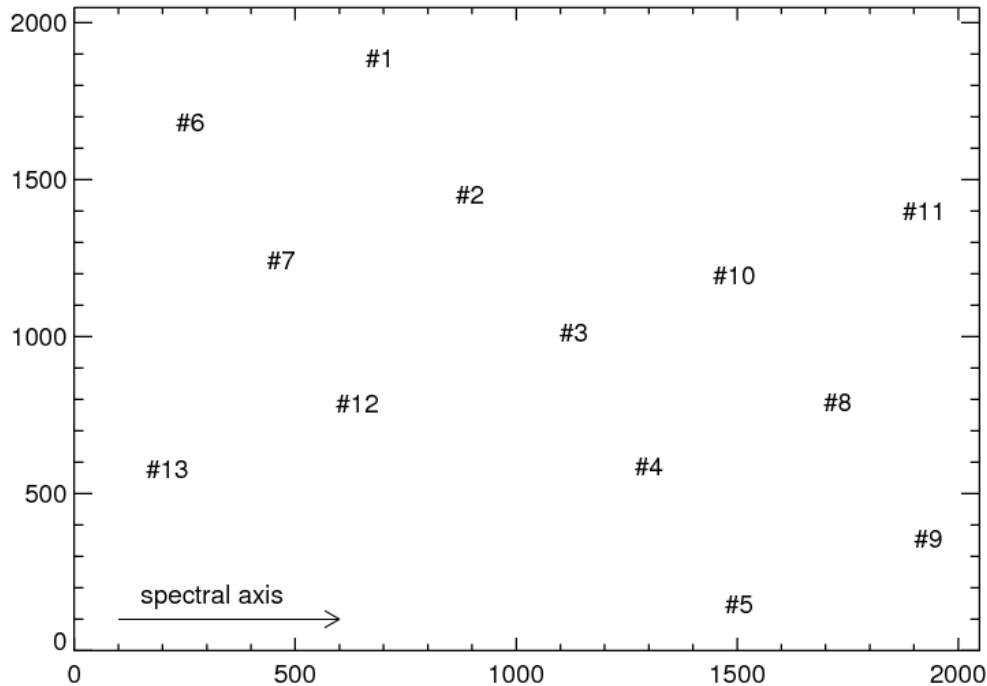


Figure 4: Pinhole grid locations on the detector.

3. EXTRACTED PARAMETERS FROM DATA

3.1 Image quality

The dataset from the focus sequence described above was analysed in the following manner. First images were dark-subtracted, we then extracted each 10x10 pinhole grid, and fitted a 2-D Gaussian on all pinholes. The FWHM for each field position was estimated from the median of Gaussian widths for each pinhole grid.

As the measured FWHM values were close to the pixel scale (as small as 1.5 pixel), we corrected for various effects. First, the Hawaii-II detectors have a non-zero pixel cross-talk. We derived the mean pixel cross-talk for this array using hot-pixels. Using a map of hot pixels, we median-combined hot pixels within the linearity limit but significantly above readout noise. The resulting map indicates that 16% of the flux received in a pixels is detected in the neighbouring pixels, most of it going to the immediately 4 adjacent pixels. The order of magnitude of this effect is consistent with the ~20% cross-talk quoted by the manufacturer. The second effect that we included is the pinholes finite size. The pinholes used here have a 5 μm diameter, corresponding to 8.5 μm ($\sim\frac{1}{2}$ pixel) on the detector considering the paraxial IFS optical magnification of 1.73274.

To determine the impact of these effects on our FWHM measurements, we produced a 10-times oversampled instrumental PSF corresponding to the pixel median cross-talk convolved by the geometric disk of the finite-sized pinholes. We convolved this instrumental PSF with Gaussian of known FWHM and binned the resulting PSF to the actual pixel size. The measured FWHM of the degraded PSF is, as expected, slightly larger than the input FWHM. This effect is small for large FWHMs (a measured 3 pixel FWHM corresponds to a 2.78 pixel true FWHM) but for the best

FHWMs measured during this test ~ 1.7 pixel, this corresponds to a ‘true’ FWHM of 1.3 pixel, a 25% correction. We produced a table for the range of measured FWHMs and corrected the measured FWHMs in the figures shown below. The resulting FWHM versus focus stage position is shown in Figure 5. These measurements show, as expected, a variation of the best focus position through the field-of-view (Figure 4). Minimizing the mean FWHM for the whole field-of-view gives a FWHM varying spatially from 21 to 26 μm (1.1-1.5 pixel).

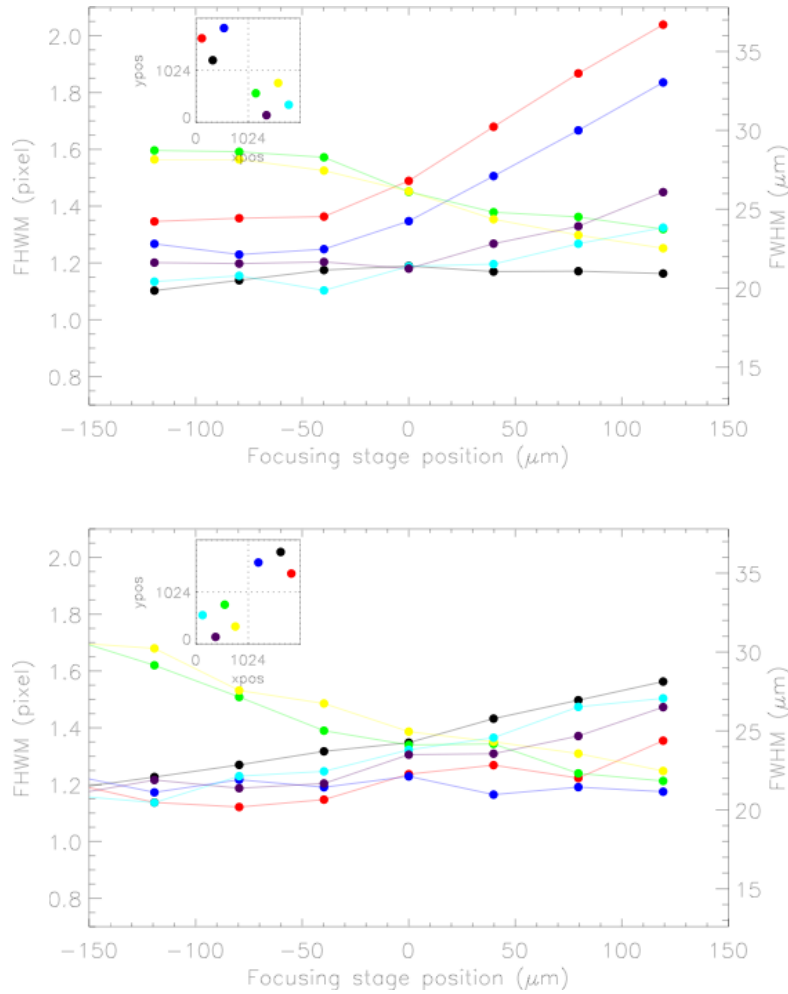


Figure 5 Full-width at half-maximum for the two detector orientations as a function of the focusing stage position. The best focus position has been defined as the zero point of the focusing stage. For the two orientations, all positions have FWHMs between 21 μm and 26 μm . The inset plots show the field positions for each FWHM curve. All FWHMs have been corrected for pixel crosstalk and pinhole size (see text).

The measured optical quality is consistent with previous tolerance analysis suggesting that FWHM better than 1.7 pixels should be expected with 90% probability or better than 1.4 pixels with 50% probability.

3.2 IFS Dispersion

The dispersion was measured and compared to the Zemax IFS model and to a linear fit. Raw images from Argon and Xenon lamps were used to extract centroid locations of pinholes PSF at 1.695um (Ar) and [1.542,1.605,1.6732,1.733] um (Xe), after dark subtraction. Distance of each peak from the 1.695 um Ar peak were calculated for each spectrum and the mean value of these distances were calculated for a given 10x10 pinhole grid.

Absolute relative difference with Zemax model and linear model are reported on the table below. Comparison between data and Zemax spectra locations were made at all field positions.

Location on detector	#1	#2	#3	#4	#5	#6	#7	#8	#9
Zemax mean Err.	3.9%	1.4%	1.9%	2.7%	2.8%	4.4%	4.2%	2.2%	1.3%
Linear fit mean Err	1.4%	0.8%	0.6%	1.0%	1.8%	2.4%	1.2%	1.0%	0.8%

This table shows a very good agreement with the IFS Zemax model and it suggests that a linear fit of the dispersion is a very good approximation. The fact that the Zemax mean error is slightly greater than the linear fit one, can be due to the uncertainties on the determination of the exact location of the reference center on the detector (optical axis) in these tests.

3.3 Tilts of spectra

Tilts of spectra with respect to the spectral axis were calculated for each spectrum using locations of peaks in Argon and Xenon lamp images. For each spectrum, a mean tilt was calculated from several locations of these peaks. Dark subtracted images from Argon and Xenon lamps were used to extract centroid locations of pinholes PSF at [1.505,1.695,1.792]um (Ar) and [1.542,1.605,1.6732,1.733] um (Xe). Then, the mean value of tilts over a square of 10x10pinholes was calculated. Difference between extracted tilts and Zemax tilts are less than 0.5 deg. The measured tilts are in excellent agreement with the optical model.

3.4 Spectral length

Length of spectra is defined here as the pixel length between 1.5 and 1.8 um, the width of the H-band filter used with the prism. Those were derived from white lamp and Xe images. Spatial derivative of white lamp images were calculated to identify the [1.5,1.8]um locations of each spectra. Comparison of spectral lengths with those given by the IFS Zemax model was made at various FOV locations. The results are reported in the table below. The agreement with the optical model prediction is excellent.

Locations on	#10	#11	#12	#13

detector				
White light spec. length (pix)	16.9	15.9	18.1	19.0
Extrapolation from Xenon wavelength solution	16.9	16.0	18.1	19.1
Zemax length (pix)	17.0	16.0	18.6	19.3

3.5 Micro-pupil orientation and spectral spacing

The micro-pupil orientation and the spectral spacing are parameters that depend on the orientation of the pinhole grid used during the tests. It should be noted that the spectral spacing calculated hereafter is not representative of final GPI IFS spectral spacing as the pinhole pitch used for the test was 100 μm instead of the nominal 110 μm lenslet pitch. The micro-pupil pattern P was calculated using micropupil locations across the FOV. A constant value of 2.06 was found the FOV, which corresponds to a micro-pupil orientation $\theta=25.8$ degrees with respect to the spectral axis. For comparison, the micro-pupil pattern found with the Zemax model is $P=1.97$ ($\theta=26.9$ deg).

The spectral spacing was calculated using micropupil locations and its value ($w=4.03$ pixels) was found to be constant across the FOV, in excellent agreement with the expected value of 4.1 from the optical model (with 100 μm pitch). The separation between two adjacent micro-pupils along the dispersion axis was found to be 21.25 pixels compared with 21.4 from the Zemax model (with 100 μm pitch).

3.6 Spectral resolution

Wavelength solutions were calculated using the GPI Data Reduction Pipeline. The DRP successfully identified the expected spectral emissions of the lamps to calculate the locations of the spectral peaks from which the dispersion was deduced. Wavelength solutions were calculated over 10x10 pinhole squares across several area of the FOV. This solution for each spectrum includes the linear dispersion coefficient and mean tilt of each spectrum with respect to the spectral axis. The following two figures represent wavelength solutions overplotted on raw Xe and Ar images.

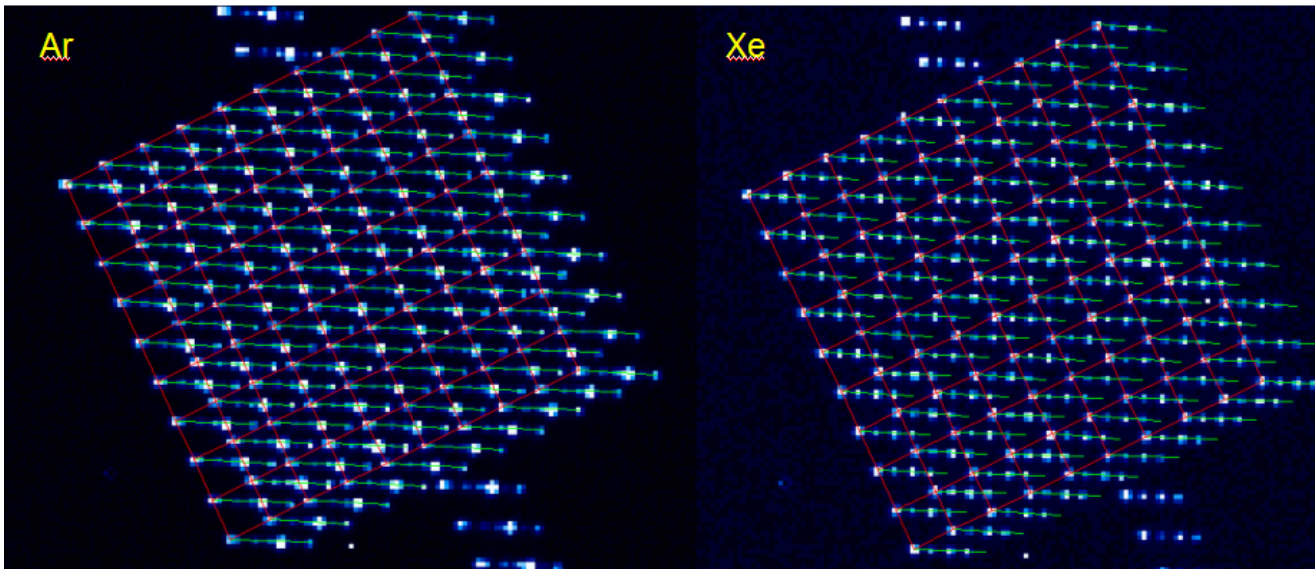


Figure 6: Examples of 2 squares of 10x10 spectra (Ar and Xe lamps) with wavelength solution grid overlotted: intersections of red lines give locations of the spectra at a given wavelength, and green segments represent calculated tilts of the spectra.

As extracted data, we represent hereafter the mean spectrum (normalized by its max value) obtained with 10x10 Xenon spectra, for several locations across the FOV. These spectra are compared to the theoretical lamp spectra on the figure hereafter.

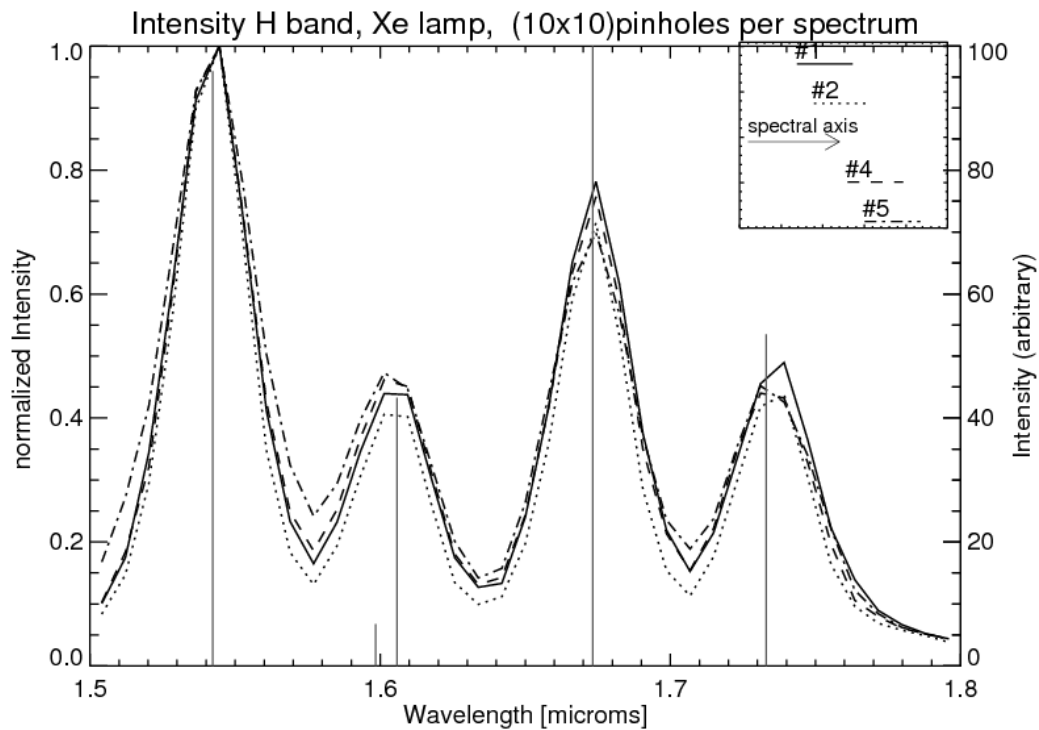


Figure 7 Spectra obtained with the Xenon lamp, dark subtracted. Each spectrum represented is the mean spectrum of

(10x10) spectra.

Spectral resolution was calculated using FWHM of spectra obtained using the laser at 1.55 μ m. Results are reported in the following table :

Locations on detector	#1	#2	#4	#5	#10	#11	#12	#13
Spectral resolution	47.2	51.0	46.3	43.6	47.7	47.3	49.0	43.8

4. CONCLUSIONS

The measured image quality, plate scale, distortion and dispersion of the IFS optics at operating temperature are in excellent agreement with the optical model. The optics experienced three cryo-cycles. The described test procedure is adequate to characterize the spectrograph optical quality.

5. ACKNOWLEDGMENTS

This work was supported by University of California (PO 1000 P KB601 01) and by NSERC.

REFERENCES

- [1] Macintosh, B., Graham, J., Palmer, D., Doyon, R., Gavel, D., Larkin, J., Oppenheimer, B., Saddlemyer, L., Wallace, J. K., Bauman, B., Evans, J., Erikson, D., Morzinski, K., Phillion, D., Poyneer, L., Sivaramakrishnan, A., Soummer, R., Thibault, S., and Veran, J.-P., "The Gemini Planet Imager," Proc. SPIE 6272, 18 (Jul 2006).
- [2] Macintosh, B. A., Graham, J. R., Palmer, D. W., Doyon, R., Dunn, J., Gavel, D. T., Larkin, J., Oppenheimer, B., Saddlemyer, L., Sivaramakrishnan, A., Wallace, J. K., Bauman, B., Erickson, D. A., Marois, C., Poyneer, L. A., and Soummer, R., "The Gemini Planet Imager: from science to design to construction," Proc. SPIE 7015, 31 (Jul 2008).